The aromatic character of [10]annulenes and dicupra[10]annulenes from current density calculations

Dimitrova, Maria

2018-01-21

Dimitrova , M & Sundholm , D 2018 , ' The aromatic character of [10]annulenes and dicupra[10]annulenes from current density calculations ' , Physical Chemistry Chemical Physics , vol. 20 , no. 3 , pp. 1337-1346 . https://doi.org/10.1039/c7cp07212k

http://hdl.handle.net/10138/309492
https://doi.org/10.1039/c7cp07212k

unspecified
acceptedVersion

Journal Name

ARTICLE TYPE

Cite this: DOI: 10.1039/xxxxxxxxxx

The aromatic character of [10]annulenes and dicupra[10]annulenes from current density calculations

Maria Dimitrova[a] and Dage Sundholm[a]

Received Date
Accepted Date

DOI: 10.1039/xxxxxxxxxx

www.rsc.org/journalname

We have investigated aromatic properties of seven low-lying isomers of [10]annulene and of the recently synthesised dicupra[10]annulene compounds that were crystallised with two or four lithium counterions (Wei *et al. J. Am. Chem. Soc.* (2016) **138** 60-63). The molecular structures of the [10]annulene conformers and the dicupra[10]annulenes with bulky trimethylsilyl (TMS) and phenyl groups, as well as the corresponding unsubstituted dicupra[10]annulenes were optimised using density functional theory, employing a semi-empirical dispersion correction to consider van der Waals interactions. The structures of the hydrocarbon annulenes were subsequently optimised at the SCS-MP2/def2-QZVPD level. Single-point coupled-cluster calculations with explicit treatment of the electron correlation CCSD(F12)(T) were performed to obtain the relative energies of the hydrocarbon annulenes. Four of the conformations lie close in energy relative to each other. Three substituted and three unsubstituted dicupra[10]annulenes structures with either four, two or no Li^+ counterions were investigated. Magnetically induced current densities calculated using the GIMIC program were used for the assessment of the aromatic properties of the studied molecules. The conformations of [10]annulene with lowest energies are non-aromatic. The calculations revealed that the electron donation of the lithium atoms to the dicupra[10]annulene core significantly affects the electronic and molecular structures of the dicupra[10]annulenes. The annulene ring is non-planar for all studied dicupra[10]annulenes except for the unsubstituted one with four Li^+ counterions, which was also found to be the only molecule that sustains a strong diatropic ring current around the dicupra[10]annulene ring. The five other dicupra[10]annulenes sustain very weak net ring currents and can be considered non-aromatic.

Introduction

Classical examples of aromatic 10 π-electron systems are naphthalene and azulene, both of which have planar geometry. The hydrocarbon [10]annulene also possesses 10 π electrons, however, it does not exhibit any strong aromatic character.[1,2] The planar all-*cis* structure suffers from bond-angle strains. Different out-of-plane conformations with more natural bond angles have been suggested in the literature based on the measured proton nuclear magnetic resonance (^{1}H NMR) spectra and computational data.[3–9] The energy differences and the barriers between the conformations are very small because the potential energy surface of [10]annulene is flat.[1]

The planarity of the [10]annulene core can be forced, for example, by introducing a methylene bridge, forming 1,6-methano[10]annulene.[5,10,11] Peaks of aromatic protons were found in the ^{1}H NMR spectrum of the bridged bicyclic molecule.[10] Therefore, one would expect that a prerequisite for aromatic properties of the dicupra[10]annulenes is a planar structure of the annulene core.

In 2015, Wei *et al.* synthesised copper-based metallanaphthalenes from substituted 1,4-dilithio-1,3-butadienes and Cu(I) salts.[12] The main product they isolated was dicupra[10]annulene with three trimethylsilyl (TMS) and three phenyl groups at the carbon atoms (Figure 1), which crystallised with four lithium counterions, two on each side of the core structure (molecule $\mathbf{B}_4$).

[a] *University of Helsinki, Department of Chemistry, P.O. Box 55, A. I. Virtasen aukio 1, FIN-00014 University of Helsinki, Finland and Centre for Advanced Study at the Norwegian Academy of Science and Letters, Drammensveien 78, N-0271 Oslo, Norway E-mail: maria.dimitrova@helsinki.fi, dage.sundholm@helsinki.fi*

† Electronic Supplementary Information (ESI) available: The ESI contains the optimised Cartesian coordinates of the studied molecules, the calculated isotropic nuclear magnetic shielding constants, induced current density profiles plots and high-resolution images of the streamline representations of the current densities of the investigated molecules. See DOI: 10.1039/b000000x/

They also found small amounts of a product coordinating only two lithium ions on one side of the annulene moiety (molecule $\mathbf{B}_2$), which was obtained in good yield using a different synthetic pathway, as reported in the same work.[12]

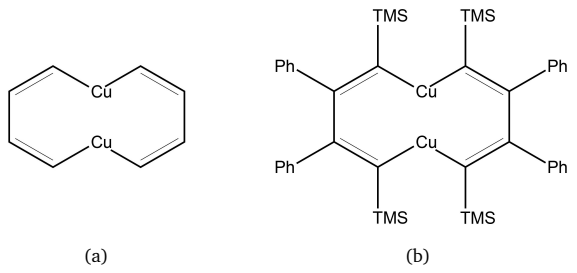

Fig. 1 Structural formula of dicupra[10]annulene (a) without substituents ($\mathbf{A}_0$) and (b) with trimethylsilyl (TMS) and phenyl groups ($\mathbf{B}_0$). The subscript index indicates the number of lithium ions coordinated to the annulene core.

The dicupra[10]annulene core possesses 8 π electrons. Each copper atom contributes a valence σ electron, hence the electronic configuration of the ten-member moiety follows the $(4n+2)$ Hückel rule for aromaticity.[13,14] However, each lithium atom in the crystalline structure donates an electron to the ring system, making structure $\mathbf{B}_2$ to 12-valence-electron system, and $\mathbf{B}_4$ has 14 valence electrons. According to the Hückel rule, $\mathbf{B}_2$ is expected to be an antiaromatic molecule with $4n$ valence electrons and $\mathbf{B}_4$ an aromatic molecule having $(4n+2)$ delocalised electrons in the ring.

Wei *et al.* performed a thorough characterisation of the synthesised copper-based annulenes. ^{7}Li NMR spectroscopy yielded chemical shifts for $\mathbf{B}_4$ that are typical for aromatic molecules.[12] The x-ray structural analysis revealed that the annulene moiety in $\mathbf{B}_4$ is close to planar, whereas in $\mathbf{B}_2$ the annulene moiety is twisted. Wei *et al.* further used computational approaches such as the isomerisation stabilisation energy (ISE) method[15] and the nucleus-independent chemical shifts (NICS) method[16,17] to assess the degree of aromaticity. The results of the computational studies also suggested that $\mathbf{B}_4$ is aromatic and $\mathbf{B}_2$ is non-aromatic.[12]

The dicupra[10]annulene with hydrogen atoms at all carbon atoms and two ($\mathbf{A}_2$) or four ($\mathbf{A}_4$) lithium ions was recently investigated computationally by Grande-Aztatzi *et al.* [18] They employed the normalised Giambiagi multicentre electron delocalisation index I_{NG} to evaluate the electron density distribution in the molecule, claiming that it is a reliable marker for the aromatic character of the molecules.[19–26] The conclusion based on their calculations was that molecule ($\mathbf{A}_4$) and naphthalene have comparable aromatic character. They further reported the NICS(0) and the NICS(0)$_{zz}$ values, both of which are more negative than the respective values for naphthalene. These results suggested that structure $\mathbf{A}_4$ is even more aromatic than naphthalene.[18]

Molecular-orbital analysis of the aromatic properties of $\mathbf{A}_2$ and $\mathbf{A}_4$ has recently been reported by An *et al.* [27] They also calculated nucleus independent chemical shifts (NICS(0)$_{zz}$) and anisotropy of the induced-current densities (ACID) functions.[17,28] The NICS(0)$_{zz}$ and ACID calculations suggested that $\mathbf{A}_4$ is aromatic and $\mathbf{A}_2$ is antiaromatic.

In this work we assess the aromatic character of the dicupra[10]annulenes by calculating magnetically induced current densities and analysing their pathways. We investigate the effect of the large substituents on the geometry and the aromatic character by studying dicupra[10]annulenes with hydrogen atoms ($\mathbf{A}_n$) at the carbon atoms as well as the corresponding molecules with trimethylsilyl (TMS) and phenyl groups substituents replacing the hydrogens ($\mathbf{B}_n$). The index n denotes to the number of lithium counterions in the molecule. The current densities are compared to those obtained for naphthalene, which is a typical 10 π-electron bicyclic aromatic molecule. We also analysed the current pathways in four conformations of [10]annulene without metal atoms, which is traditionally considered to be a non-aromatic molecule.

The paper is structured as follows. After we introduced the scientific problem and a brief discussion of previous studies on the dicupra[10]annulenes, we describe in the next section the computational tools that we have employed. Then, we present computational procedures in more detail and discuss the obtained results. The main conclusion are drawn in the last section.

Computational methods

The molecular structures of the dicupra[10]annulenes and naphthalene were optimised at the density functional theory (DFT) level with TURBOMOLE employing the BP86 density functional and the triple-ζ def2-TZVP basis set with Grimme's D3-BJ dispersion correction.[29–38] The optimisation of the molecular geometries was speeded up by using the resolution-of-the-identity (RI) approximation.[39] The structures of a few conformers of [10]annulene were optimised at the B3LYP/def2-TZVP/D3-BJ and SCS-MP2/def2-QZVPD levels of theory.[40–47] Single-point calculations were performed at the explicitly correlated coupled-cluster singles and doubles level with a perturbative treatment of the triples using the F12 ansatz (CCSD(F12)(T)). The CCSD(F12)(T)/def2-TZVP calculations correspond to CCSD(T) calculations close to the basis set limit.[48–55] The optimised SCS-MP2/def2-QZVPD structures were used in the CCSD(F12)(T)/def2-TZVP calculations. Zero-point energy contributions and entropy effects were estimated by performing B3LYP/def2-TZVP/D3-BJ calculations of the vibrational energies using the AOFORCE module of Turbomole.[56] The m5 integration grid was used in the DFT calculations.[57]

The nuclear magnetic shielding calculations were performed at the B3LYP/def2-TZVP level of theory.[32,33,35–37,58] The geometry and basis set data, as well as the unperturbed and magnetically perturbed density matrices were used as input to the GIMIC program.[59]

GIMIC is an open-source program for visualisation and numerical integration of the magnetically induced current density susceptibilities in the limit of zero external magnetic field for open- and closed-shell molecules. The current densities depend on the strength of the external magnetic field multiplied with the current density susceptibility. In the discussion, we refer to them as *current densities* for simplicity. Current-strength susceptibilities

(*current strengths*) can be obtained by performing integration of the current density that passes planes positioned perpendicularly to the molecular plane. Integration planes can begin at the ring centre and then cross a chemical bond or pass through an atom. The end of the integration plane is far away from the molecule, where the current density vanishes. For practical purposes the integration can end 10 bohr away from the chemical bond as well as 10 bohr above and below the molecular plane. The integration yields the induced current densities going in diatropic or paratropic direction, as well as the net current strength passing the integration plane.

Rationalisation of the strength of the various induced current loops can quantitatively be done by splitting the integration plane into thin slices that are for example 0.02 bohr wide. The current strength is obtained by adding the current contributions from the thin slices. Plotting the integrated current strength of the individual slices as a function of the position of the slices yields the profile of the current density passing the integration plane. *Current density profiles* consist of separate domains corresponding to *local currents* which include *atomic*, *bond*, and *ring currents*. The *global current* flows along the perimeter of the whole molecule. In complicated polycyclic molecular systems, there may be *semi-local currents* which flow around several molecular rings but not around the entire molecule. Further details on the GIMIC method and its applications are provided in the extensive review by Sundholm *et al.* [60]

Qualitative inspection of the induced current pathways can be done with a streamline representation of the current-density vector field calculated on a 3D numerical grid. The visualisation of the current density assists the choice of integration planes for quantitative analysis. The images were obtained by applying the line integral convolution (LIC) plugin in Paraview with a colour scheme corresponding the current strength.[61] Current profiles calculated in planes that are perpendicular to the molecular plane and integration of the individual current strength contributions reveal what is the current-density flow in the molecule. This technique was recently employed to rationalise the complicated pathways in polycyclic molecules.[62] VMD and GIMP are other tools that we use for creating graphics.[63,64]

Results

Naphthalene

Even though the aromatic character of naphthalene has been previously studied by many research groups,[17,60,65–71] we also investigate it with the same tools as we use in the dicupra[10]annulene study. Based on the visual analysis of the streamline plots, we identified paratropic ring currents in the six-member rings, and a global current looping around the whole molecule. A notable feature is the current density in the π orbitals at the central bond between the C5 and C10 atoms (Figures 2 and 3). The bond current in the C5–C10 bond is significantly stronger than the bond current in the C–C bonds of benzene or in the C–C bonds of the perimeter of naphthalene. The current vortex of the shared bond persists far away from the molecular plane, in contrast to typical σ bond currents that vanish at about 1 bohr from the molecular plane.

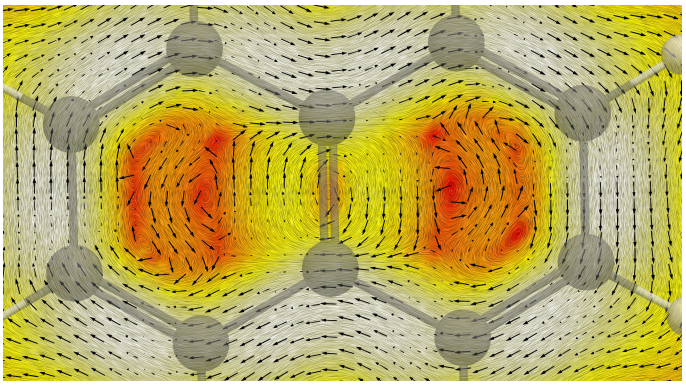

Fig. 2 LIC representation of the current density 1.5 bohr from the molecular plane of naphthalene.

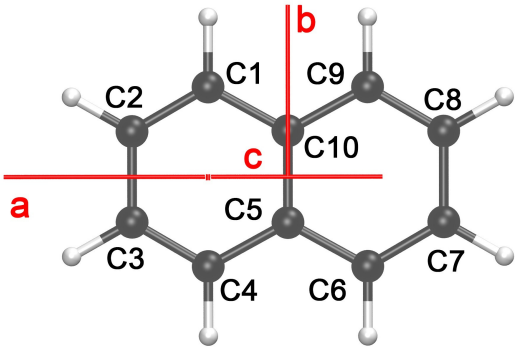

Fig. 3 Labels of the integration planes used in the analysis of the current density in naphthalene.

The current flow 1.5 bohr above the molecular plane is visualised in Figure 2. It is shown in greater detail in the electronic supplementary information (ESI).† Three integration planes were used for the rationalisation of the induced current strengths as shown in Figure 3. Plane **a** begins at the ring centre and plane **b** begins at the centre of the C5–C10 bond. They both extend far outside the molecule. Plane **c** goes from ring centre to ring centre. The net current strengths as well as the diatropic and paratropic contributions are given in Table 1.

Table 1 The magnetically induced current strengths (in nA/T) passing planes **a**, **b** and **c** in naphthalene.

Plane	Net	Diatropic	Paratropic
a	12.60	17.61	-4.99
b	21.18	30.47	-9.13
c	0.00	7.74	-7.74

[10]annulene

Based on the benzene structure, a first guess for the molecular structure of [10]annulene would be the all-*cis* conformation. However, this structure was discarded already in the early predictions of its molecular geometry.[3] Other conformations have been suggested based on experimental data and on calculations at fairly low levels of theory. In more recent calculations at the CCSD(T)/DZd level of theory,[8] King *et al.* identified three confor-

mations of [10]annulene with relative energy differences of less than 5 kcal/mol. The structures are shown in Figure 4. Here, we adopted the reported structures and re-optimised them at the SCS-MP2/def2-QZVPD level of theory. The obtained structures agree well with the ones for the conformers investigated by King *et al.* The root-mean-square deviation (RMSD) for the structures are only 0.03–0.09 Å. Structural optimisations at the B3LYP/def2-TZVP/D3-BJ level yielded RMSD deviations of 0.01–0.05 Å from the structures obtained at the SCS-MP2/def2-QZVPD level. Relative energies were obtained by performing single-point calculations at the CCSD(F12)(T)/def2-TZVP level using the SCS-MP2/def2-QZVPD structures. Free-energy differences were obtained at T=298.15 K by calculating vibrational effects at the B3LYP/def2-TZVP/D3-BJ level corrected for rotational and translational contributions estimated at classical level of theory.

At DFT level the planar all-*cis* conformer has two imaginary vibrational frequency, suggesting that it is a transition state. This conformer is a transition state between mirror images of the reported minima. By moving atoms along the imaginary vibrational modes we obtained different slightly bent structures. Some of them are shallow local minima and consecutive distortions of the structures lead to the low-lying twist and boat conformers. The five structures studied by King *et al.* lie within 6 kcal/mol relative to each other at the CCSD(T) level. By considering zero-point vibrational energies and entropy effects calculated at room temperature, the energy difference increases to 7 kcal/mol. The small energy differences suggest that transitions from one conformer to the other can occur at ambient temperature. The energies at the CCSD(F12)(T) level of theory set the conformers in following order of decreasing energy: twist < naphthalene-like < heart-shaped < boat < azulene-like. The obtained trend largely agrees with the findings of King *et al.* ,[8] who concluded that the boat conformer is more stable than the heart-shaped one.

The most stable conformer is a non-planar twisted structure. It sustains a weak ring current of 0.58 nA/T, showing that it is non-aromatic. The naphthalene-like conformation lies 1.6 kcal/mol higher in energy. It exhibits a global diatropic current of 9.73 nA/T that is almost cancelled by the global paratropic current yielding a net ring current of only 2.91 nA/T. The heart-shaped conformation is the least stable structure of the three. It is nearly planar, with one hydrogen pointing inwards to the centre of the ten-member ring. It is strongly aromatic with a net ring current of 17.32 nA/T, which is in agreement with the findings by Sulzbach *et al.* [6,7] However, the existence of the heart-shaped structure has not been confirmed experimentally. The azulene-like conformation is about 1.0 kcal/mol higher in energy than the heart-shaped conformation and it is also aromatic. The boat conformation lies energetically between the heart-shaped and the azulene-like structures. The all-*trans* [10]annulene is an interesting structures that have not been observed in laboratory conditions.[72] The all-*cis* conformer lies high in energy and is a planar transition state. It is aromatic and sustains a net current of 19.36 nA/T. The all-*trans* conformer exhibits in-plane conjugation, with the π orbitals pointing inwards and outwards. Current density calculations show that it is strongly aromatic, sustaining a ring current of 14.90 nA/T. It is noteworthy that unlike usual cyclic molecules, the all-*trans* conformer does not exhibit any significant paratropic ring current. The experimentally known isomers of [10]annulene are non-aromatic,[1] whereas the heart-shaped, the all-*cis* and the all-*trans* conformers are aromatic according to the present calculations. Current profiles and streamline visualisations of the current densities are provided in the ESI.†

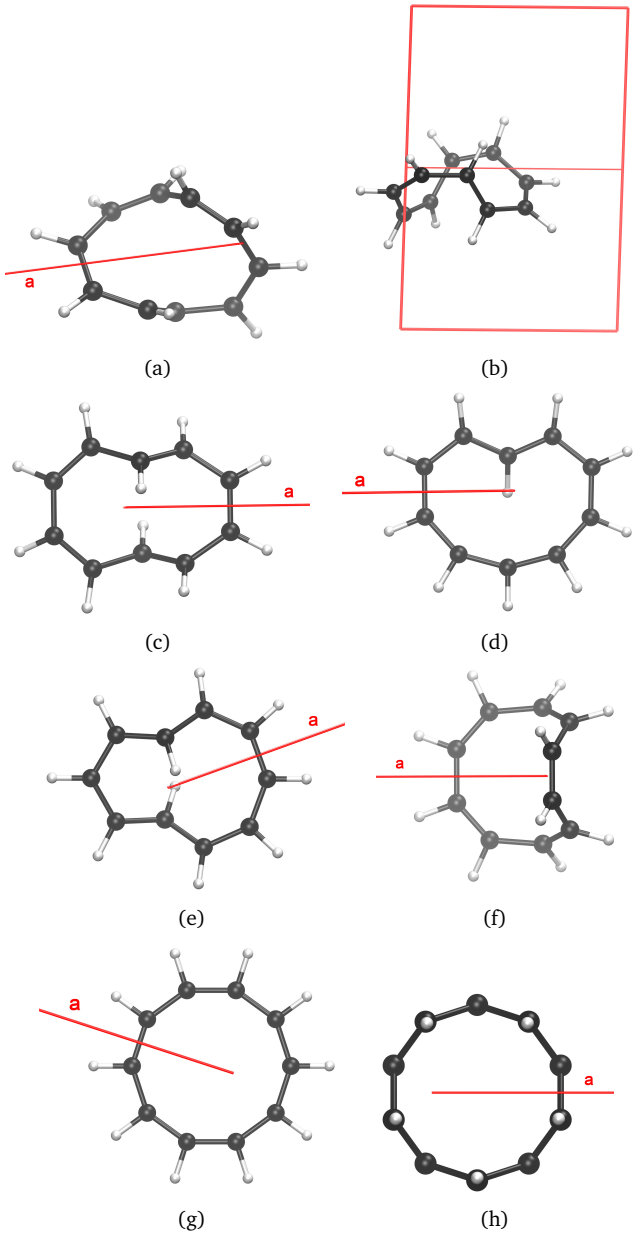

Fig. 4 The molecular structures of five low-lying conformers of [10]annulene as well as of the all-*trans* and the all-*cis* conformations. (a) twist, top view; (b) twist, side-view; (c) naphthalene-like; (d) heart-shaped; (e) azulene-like; (f) boat; (g) all-*cis* ; (h) all-*trans* .

Table 2 Relative energies (ΔE in kcal/mol) of the investigated [10]annulene conformers as obtained in CCSD(F12)(T)/def2-TZVP calculations with the molecular structures optimised at the SCS-MP2/def2-QZVPD level. The zero-point energies (ZPE) and vibrational entropy contributions to the Gibbs free energy (ΔG in kcal/mol) at 298.15 K were calculated at the B3LYP/def2-TZVP/D3-BJ level of theory. The translational and rotational entropy contributions to the free energy were obtained classically.

Molecule	ΔE	ZPE+Entropy	ΔG
twist	0.00	0.00	0.00
naphthalene-like	1.02	0.56	1.58
heart-shaped	3.46	1.54	5.00
azulene-like	6.04	0.95	6.99
boat	5.42	-0.27	5.15
cis [a]	26.40	4.34	30.74
trans	79.01	-0.25	78.76

[a] Transition state structure with two imaginary frequencies.

Table 3 The magnetically induced current strengths (in nA/T) passing the integration planes in the investigated conformers of [10]annulene.

Conformer	Net	Diatropic	Paratropic
twist	0.58	3.41	-2.82
naphthalene-like	2.91	9.73	-6.84
heart-shaped	17.32	21.87	-4.55
azulene-like	13.80	18.60	-4.95
boat	0.58	7.57	-6.39
all-*cis* [a]	19.36	23.90	-4.23
all-*trans*	14.90	16.41	-1.52

[a] Transition state structure with two imaginary frequencies.

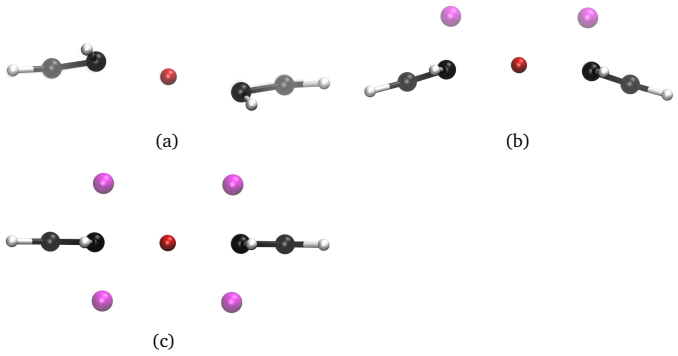

Fig. 5 Side view of the dicupra[10]annulenes without bulky substituents and (a) no lithium ions ($\mathbf{A}_0$), (b) two lithium ions ($\mathbf{A}_2$) and (c) four lithium ions ($\mathbf{A}_4$). The carbons are shown in black, hydrogens are white, coppers are red, and lithiums are pink.

Dicupra[10]annulenes

We have investigated dicupra[10]annulenes with hydrogen atoms at the carbon atoms ($\mathbf{A}_0$, $\mathbf{A}_2$, $\mathbf{A}_4$), as well as with phenyl and TMS groups as substituents ($\mathbf{B}_0$, $\mathbf{B}_2$, $\mathbf{B}_4$). The structures are shown in Figure 1. The number of lithium ions (n) plays an important role for the structure and aromaticity of the dicupra[10]annulenes as pointed out by Wei *et al.* [12] Each lithium atom donates one electron to the dicupra[10]annulene core, which affects its aromatic character. In the absence of bulky substituents, the hydrocarbon fragments consisting of four CH groups are planar in all three $\mathbf{A}_n$ molecules. However, the hydrocarbon fragments tilt relatively to each other. The tilting angle depends on the number of Li^+ ions. A side view of the molecules is shown in Figure 5. The dihedral angles are listed in Table 4.

Table 4 Selected dihedral angles in degrees (°) as labelled in Figure 6

Molecule	Angle 1	Angle 2	Angle 3	Angle 4
$\mathbf{A}_0$	−0.2	52.4	178.4	22.6
$\mathbf{A}_2$	0.0	0.1	171.6	15.3
$\mathbf{A}_4$	0.0	0.0	180.0	0.1
$\mathbf{B}_0$	−0.3	−70.9	−87.9	−91.1
$\mathbf{B}_2$	20.5	−95.8	130.3	−36.6
$\mathbf{B}_4$	8.3	−58.0	−154.4	−25.0

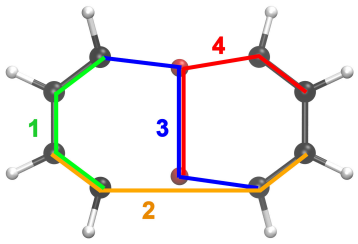

Fig. 6 The labels of the dihedral angles listed in Table 4.

Unsubstituted dicupra[10]annulene

Based on visual inspections of the current density loops and vortices, we defined three integration planes, shown in Figure 7. The same integration planes were chosen as for naphthalene. Since there is no vortex at the centre of the six-membered ring, plane **c** is replaced by extending plane **a** to the center of the molecule (**a***). The calculated current strengths crossing the selected integration planes are given in Table 5. There is a very strong atomic current around the copper atoms, which one might expect for heavy elements with a large number of electrons. Atomic currents for carbon atoms usually are weaker than 2 nA/T, whereas for copper we obtained diatropic atomic currents that are up to two orders of magnitude stronger.

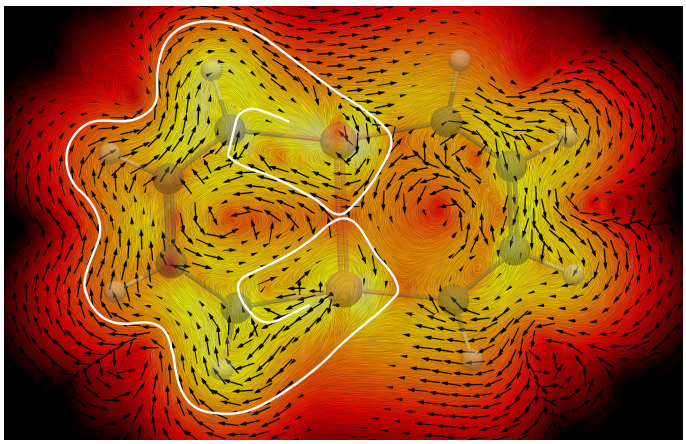

Fig. 7 The integration planes used in the current density analysis of the dicupra[10]annulenes are shown in red.

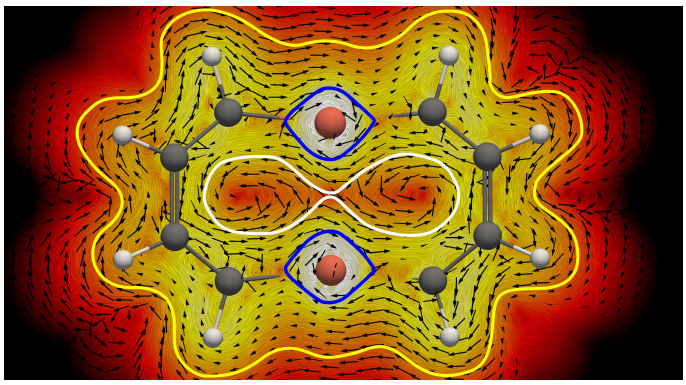

Fig. 8 LIC representation of the current density 1.0 bohr from the base plane in molecule $\mathbf{A}_0$. The white curve illustrates the semi-local current pathway on one side of the molecule.

Table 5 The magnetically induced current strengths (in nA/T) in the unsubstituted dicupra[10]annulenes ($\mathbf{A}_0$, $\mathbf{A}_2$ and $\mathbf{A}_4$) calculated at the B3LYP/def2-TZVP level of theory. Plane **a*** begins in the midpoint between the copper atoms.

Molecule	Plane	Net	Diatropic	Paratropic
$\mathbf{A}_0$	**a**	4.57	10.17	-5.75
$\mathbf{A}_0$	**c**	0.00	3.86	-3.86
$\mathbf{A}_2$	**a**	-0.13	9.33	-9.46
$\mathbf{A}_2$	**a***	0.32	11.69	-11.37
$\mathbf{A}_4$	**a***	15.13	28.12	-12.98

The streamline plots for molecule $\mathbf{A}_0$ reveal a global current surrounding the whole molecule and local paratropic ring currents flow in the six-member rings. Semi-local current loops flow around the hydrocarbon fragments and join the atomic currents of the copper atoms. The semi-local currents are illustrated in white in Figure 8. The current profiles and the streamline plots are shown in more detail in the ESI.†

In molecule $\mathbf{A}_2$, local paratropic ring currents, global paratropic and global diatropic currents were identified as shown in Figure 9. The base plane is defined by the atoms C1, C4, C5, and C8. The Cu atoms exhibit strong atomic currents, which do not expand towards the carbon atoms as in molecule $\mathbf{A}_0$. The strong diatropic and paratropic currents passing plane **b** are due to the strong atomic current of the Cu atom.

The vortex of the ring current above the six-member rings becomes distorted by the atomic currents that flow around the Li^+ ions. Thus, for $\mathbf{A}_2$ and $\mathbf{A}_4$ the net current strength passing plane **a**, which extends from the centre of the six-membered ring to infinity, does not comprise the whole global ring current. The problem can, to some extent, be circumvented by integrating the net current strength passing plane **a***, which has its origin at the midpoint between the copper atoms. The profile of the current density passing plane **a*** is shown in Figure 10.

The current pathways in the planar $\mathbf{A}_4$ molecule are practically the same as for molecule $\mathbf{A}_2$. However, the induced current strengths are larger as seen in Table 5. Molecule $\mathbf{A}_2$ is non-aromatic sustaining a very weak ring current. Molecule $\mathbf{A}_4$ is aromatic sustaining a net ring current of 15.13 nA/T, which is comparable to the net current strength of 12.60 nA/T passing plane **a** in naphthalene. For comparison, the ring-current strength of

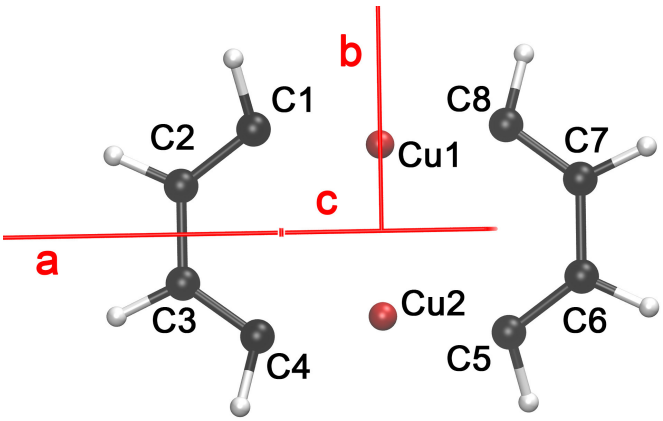

Fig. 9 LIC representation of the current density in the base plane of molecule $\mathbf{A}_2$. The lithium ions are on the opposite side of the base plane. The global diatropic current is drawn in yellow, while the global paratropic ring current is given in white. The atomic currents around the Cu atoms are illustrated with the blue loop.

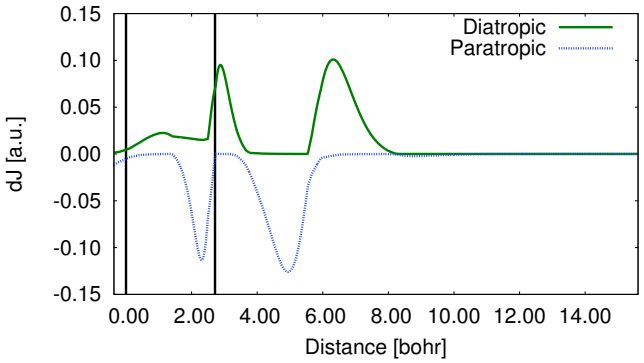

Fig. 10 The current strength profile for plane **a*** in molecule $\mathbf{A}_2$ obtained at the B3LYP/def2-TZVP level of theory. The origin is at the midpoint between the copper atoms. The geometrical centre of the six-member ring is marked with a vertical black line at a distance of 2.71 bohr from the midpoint.

benzene is 11.66 nA/T at the same level of theory.

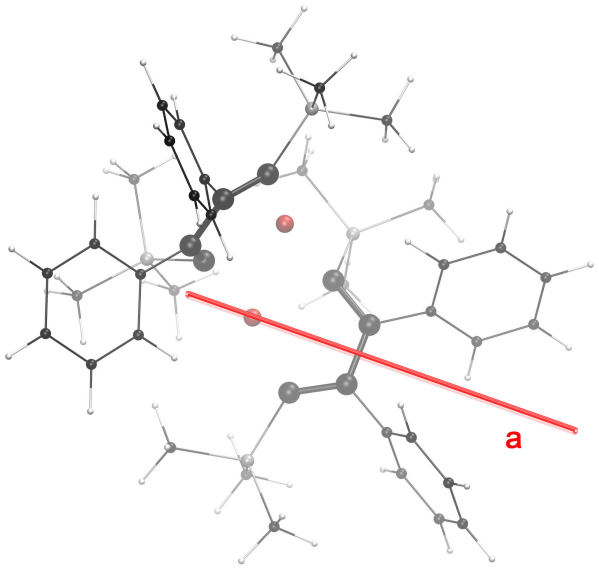

Fig. 11 The integration plane used in the current density analysis of the substituted dicupra[10]annulene without lithium ions ($\mathbf{B}_0$) seen from above is marked as a red line.

Substituted dicupra[10]annulenes

The phenyl and trimethylsilyl substituents significantly distort the annulene core structure. The bulky substituents also complicate the choice of integration planes, rendering precise determinations of the current strengths difficult. The obtained ring-current strengths are given in Table 6. Current profile plots are provided in the ESI.†

Molecule $\mathbf{B}_0$ was oriented such that one of the hydrocarbon moieties and one of the copper atoms lies in a plane perpendicularly to the external magnetic field. The integration plane was chosen according to Figure 11. The dicupra[10]annulene core of molecule $\mathbf{B}_2$ is significantly distorted. We examined the streamline representations of the current density in the molecule but we did not find any indication of a paratropic ring current, nor of any currents circulating along the perimeter of the annulene core. The integration plane was positioned as shown in Figure 12. In molecule $\mathbf{B}_4$ the current density visually resembles the ones obtained for $\mathbf{A}_2$ and $\mathbf{A}_4$. We identified paratropic ring currents and diatropic current flowing along the perimeter of the annulene core. The integration plane was positioned as shown in Figure 13.

Table 6 The magnetically induced current strengths (in nA/T) passing plane **a** in the substituted dicupra[10]annulenes ($\mathbf{B}_0$ and $\mathbf{B}_4$).

Molecule	Net	Diatropic	Paratropic
$\mathbf{B}_0$	-4.1	5.0	-9.1
$\mathbf{B}_2$	1.2	5.4	-4.2
$\mathbf{B}_4$	1.2	11.3	-10.1

In molecule $\mathbf{B}_0$ the net current is about -4 nA/T suggesting that it is non-aromatic or very weakly antiaromatic. It is nearly impossible to choose the integration plane such as it does not cross any current vortices belonging to the bulky substituents. In the current density profile, there is a domain corresponding to a diatropic ring current of 5.0 $\pm$ 0.3 nA/T and a domain inside the ring that yields a paratropic ring-current contribution of -9.1 nA/T.

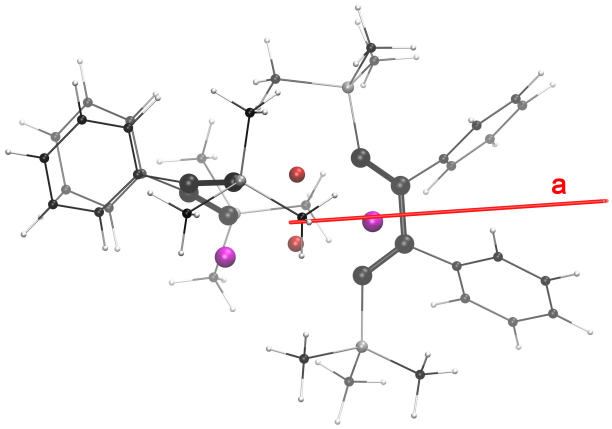

Fig. 12 The integration plane used in the current density analysis of the substituted dicupra[10]annulene without lithium ions ($\mathbf{B}_2$) seen from above is marked as a red line.

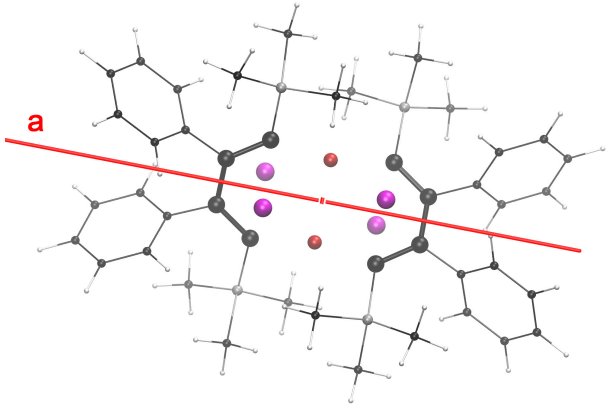

Fig. 13 The integration plane used in the current density analysis of the substituted dicupra[10]annulene without lithium ions ($\mathbf{B}_4$) is marked as a red line.

In molecules $\mathbf{B}_2$ and $\mathbf{B}_4$ the current density profiles consist of multiple overlapping domains and integrating them separately was not feasible. We identified overlapping peaks corresponding to the global diatropic and paratropic ring currents and estimated the area as peak height times the peak width at the half of its height. The obtained values are given in Table 6. The annulene core of molecule $\mathbf{B}_2$ is very twisted as seen in Figure 14a. Weak diatropic and paratropic ring currents of 5.4 nA/T and -4.2 nA/T were obtained, yielding an almost vanishing net ring-current strength. In molecule $\mathbf{B}_4$, the strength of the diatropic and paratropic contributions is about $\pm$10 nA/T leading again to a very weak net current strength. Thus, $\mathbf{B}_2$ and $\mathbf{B}_4$ are non-aromatic.

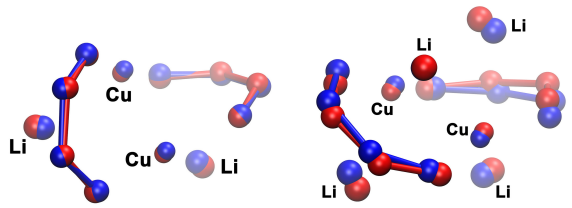

(a) (b)

Fig. 14 Comparison of the experimental x-ray structure for the substituted molecules (a) $\mathbf{B}_2$ and (b) $\mathbf{B}_4$ (in red) with the molecular structure optimised at the BP86/def2-TZVP/D3-BJ level of theory (blue). The substituents are hidden for clarity. The root-mean-square deviations of the atomic positions of the atoms of the annulene core structure are 1.05 Åand 2.12 Å for $\mathbf{B}_2$ and $\mathbf{B}_4$, respectively.

Discussion

Our computational studies reveal that [10]annulene is an interesting molecule for which several different conformations were investigated. The most stable ones, trans and naphthalene-like, are non-planar sustaining very weak net ring currents. The nearly planar heart-shaped, the azulene-like, the all-*cis* and the all-*trans* conformers are aromatic since they sustain strong diatropic ring currents. The all-*cis* conformation was found to be a transition state. The all-*cis* and all-*trans* conformers lie much higher in energy than the other five structures.

The present study suggests that in the absence of lithium ions ($\mathbf{A}_0$), the hydrocarbon fragments are individually planar but tilted with respect to each other. Only molecule $\mathbf{A}_4$ with four Li^+ counterions was found to be planar. Grande-Aztatzi *et al.* claimed that the annulene structures without substituents exhibit little deviation from the geometry in the substituted molecules.[18] However, this does not hold for $\mathbf{A}_4$ and $\mathbf{B}_4$. The planar unsubstituted $\mathbf{A}_4$ structure does not represent the experimental $\mathbf{B}_4$ structure very well, since the rings in $\mathbf{B}_4$ are twisted as shown in Figure 14. Some of the dihedral and bond angles are listed in Table 4.

The delocalisation indices calculated by Grande-Aztatzi *et al.* [18,73] indicate that there is a covalent Cu–Cu bond in molecule $\mathbf{A}_4$. However, we did not find a bond current vortex between the copper atoms that would indicate a chemical bond. In $\mathbf{A}_0$, there appears to be a very small vortex between the Cu–Cu atoms, which based on the current density scale employed in the streamline plots is so weak that its current strength is difficult to determine numerically. Based on the reported values for Cu–Cu bond lengths in the literature,[74–76] the distance between the copper atoms is somewhat too long for a Cu–Cu bond. Detailed visual representations of the induced current densities between the copper atoms, as well as Cu–Cu distances are reported in the ESI.† In order to check whether there is a Cu–Cu bond, we applied the external magnetic field along the molecular plane but perpendicularly to the Cu–Cu moiety. In the presence of a Cu–Cu bond, one expects a current vortex between the Cu atoms, which is typical for σ bonds. However, no bond current vortices between the Cu atoms are seen for any of the dicupra[10]annulenes suggesting that there is no Cu–Cu bond in the studied molecules. The observed weak local paratropic currents arise not because of a Cu–Cu bond vortex but because the atomic currents around the copper atoms occupy a large volume. The vortices nearly touch each other but do not merge.

Our calculations show that $\mathbf{A}_4$ sustains a net ring current of 15.13 nA/T suggesting that it is aromatic, which is in agreement with with the results obtained by An *et al.* [27] The GIMIC calculations show that $\mathbf{A}_2$ is non-aromatic sustaining a net ring current of 0.32 nA/T, because the diatropic and paratropic contributions are almost the same and cancel. Thus, the large positive $NICS(0)_{zz}$ values obtained for $\mathbf{A}_2$ are not due to a net paratropic ring current as suggested by An *et al.* [27]

Conclusions

The lithium counterions, which are present in the experimental structures, play an important role for the molecular structure of the dicupra[10]annulene core, because they donate electrons to the annulene moiety. The calculations show that the dicupra[10]annulene core is planar only in the unsubstituted molecule with hydrogens bound to the carbons when it is surrounded by four lithium counterions ($\mathbf{A}_4$). The unsubstituted dicupra[10]annulene rings surrounded by two or no Li^+ cations ($\mathbf{A}_2$ and $\mathbf{A}_0$) are non-planar. Steric effects from the bulky trimethylsilyl and phenyl substituents deform the dicupra[10]annulene ring in the studied molecules with four, two and without Li^+ counterions ($\mathbf{B}_4$, $\mathbf{B}_2$ and $\mathbf{B}_0$). The obtained molecular structures suggest that $\mathbf{A}_4$ is the only aromatic molecule among the six studied dicupra[10]annulenes.

The degree of aromaticity of the dicupra[10]annulenes was estimated by performing current density calculations using the GIMIC method. For comparison, current densities and current strengths were calculated at the same level of theory for naphthalene and [10]annulene. Naphthalene is a typical 10 π-electron system sustaining diatropic net current, which correlates with its aromatic character. An unexpected but weak vortex for π electrons was found around the central bond of naphthalene.

Current density calculations on the dicupra[10]annulenes with TMS and phenyl substituents show that they sustain very weak ring currents in the [10]annulene ring. For $\mathbf{B}_0$, the net ring current strength is -4.1 nA/T corresponding to a very weakly antiaromatic or practically non-aromatic system. The ring-current strengths of the non-aromatic $\mathbf{B}_2$ and $\mathbf{B}_4$ molecules are 1.2 nA/T. The corresponding molecules with the large substituents replaced by hydrogens ($\mathbf{A}_0$, $\mathbf{A}_2$, $\mathbf{A}_4$) sustain ring currents of 4.57 nA/T, 0.32 nA/T and 15.13 nA/T when they are exposed to an external magnetic field perpendicularly to the molecular ring plane. The dicupra[10]annulene core is aromatic only for the planar molecule $\mathbf{A}_4$. The calculations show that there is no Cu–Cu bond in any of the studied molecules. The obtained ring-current pathways show that the molecules are ten-member macrocyclic systems, rather than two fused six-member rings like naphthalene.

Acknowledgments

This work was supported by Magnus Ehrnrooth Foundation and by The Academy of Finland through projects 275845 and 309394. The authors acknowledge CSC – IT Center for Science, Finland and the Finnish Grid and Cloud Infrastructure (FGCI) for compu-

tational resources.

References

1 R. D. Kennedy, D. Lloyd and H. McNab, *J. Chem. Soc. Perkin Trans. 1*, 2002, 1601–1621.

2 F. Sondheimer, *Acc. Chem. Res.*, 1972, **5**, 81–91.

3 S. Masamune and R. Seidner, *J. Chem. Soc. D: Chem. Commun.*, 1969, 542–544.

4 S. Masamune, K. Hojo, K. Hojo, G. Bigam and D. L. Rabenstein, *J. Am. Chem. Soc.*, 1971, **93**, 4966–4968.

5 S. Masamune and N. Darby, *Acc. Chem. Res.*, 1972, **5**, 272–281.

6 H. M. Sulzbach, P. von Ragué Schleyer, H. Jiao, Y. Xie and H. F. Schaefer, *J. Am. Chem. Soc.*, 1995, **117**, 1369–1373.

7 H. M. Sulzbach, H. F. Schaefer, W. Klopper and H. P. Lüthi, *J. Am. Chem. Soc.*, 1996, **118**, 3519–3520.

8 R. A. King, T. D. Crawford, J. F. Stanton and H. F. Schaefer, *J. Am. Chem. Soc.*, 1999, **121**, 10788–10793.

9 C. Castro, W. L. Karney, C. M. McShane and R. P. Pemberton, *J. Org. Chem.*, 2006, **71**, 3001–3006.

10 E. Vogel, *Isr. J. Chem.*, 1980, **20**, 215–224.

11 G. F. Caramori, K. T. de Oliveira, S. E. Galembeck, P. Bultinck and M. G. Constantino, *J. Org. Chem.*, 2007, **72**, 76–85.

12 J. Wei, Y. Zhang, Y. Chi, L. Liu, W.-X. Zhang and Z. Xi, *J. Am. Chem. Soc.*, 2016, **138**, 60–63.

13 E. Hückel, *Grundzüge der Theorie ungesättigter und aromatischer Verbindungen*, Verlag Chemie, Berlin, 1938.

14 W. von Eggers Doering and F. L. Detert, *J. Am. Chem. Soc.*, 1951, **73**, 876–877.

15 P. von Ragué Schleyer and F. Pühlhofer, *Org. Letters*, 2002, **4**, 2873–2876.

16 Z. Chen, C. S. Wannere, C. Corminboeuf, R. Puchta and P. von Ragué Schleyer, *Chem. Rev.*, 2005, **105**, 3842–3888.

17 P. von Ragué Schleyer, C. Maerker, A. Dransfeld, H. Jiao and N. J. R. van Eikema Hommes, *J. Am. Chem. Soc.*, 1996, **118**, 6317–6318.

18 R. Grande-Aztatzi, J. M. Mercero, E. Matito, G. Frenking and J. M. Ugalde, *Phys. Chem. Chem. Phys.*, 2017, **19**, 9669–9675.

19 M. Giambiagi, M. S. de Giambiagi, C. D. dos Santos Silva and A. P. de Figueiredo, *Phys. Chem. Chem. Phys.*, 2000, **2**, 3381–3392.

20 J. Cioslowski, E. Matito and M. Solá, *J. Phys. Chem. A*, 2007, **111**, 6521–6525.

21 F. Feixas, E. Matito, J. Poater and M. Solá, *Chem. Soc. Rev.*, 2015, **44**, 6434–6451.

22 P. Bultinck, M. Rafat, R. Ponec, B. Van Gheluwe, R. Carbó-Dorca and P. Popelier, *J. Phys. Chem. A*, 2006, **110**, 7642–7648.

23 E. Matito, *Phys. Chem. Chem. Phys.*, 2016, **18**, 11839–11846.

24 J. M. Mercero, E. Matito, F. Ruipèrez, I. Infante, X. Lopez and J. M. Ugalde, *Chem. Eur. J.*, 2015, **21**, 9610–9614.

25 F. Feixas, J. O. C. Jiménez-Halla, E. Matito, J. Poater and M. Solá, *J. Chem. Theory Comput.*, 2010, **6**, 1118–1130.

26 F. Feixas, E. Matito, M. Duran, J. Poater and M. Solá, *Theo. Chem. Acc.*, 2011, **128**, 419–431.

27 K. An, T. Shen and J. Zhu, *Organometallics*, 2017, **36**, 3199–3204.

28 D. Geuenich, K. Hess, F. Köhler and R. Herges, *Chem. Rev.*, 2005, **105**, 3758–3772.

29 R. Ahlrichs, M. Bär, M. Häser, H. Horn and C. Kölmel, *Chem. Phys. Letters*, 1989, **162**, 165–169.

30 F. Furche, R. Ahlrichs, C. Hättig, W. Klopper, M. Sierka and F. Weigend, *WIREs Comput. Mol. Sci.*, 2014, **4**, 91–100.

31 *TURBOMOLE V7.1 2016, a development of University of Karlsruhe and Forschungszentrum Karlsruhe GmbH, 1989-2007, TURBOMOLE GmbH, since 2007; available from* `http://www.turbomole.com`.

32 A. D. Becke, *Phys. Rev. A*, 1988, **38**, 3098–3100.

33 A. D. Becke, *J. Chem. Phys.*, 1993, **98**, 5648–5652.

34 J. P. Perdew, *Phys. Rev. B*, 1986, **33**, 8822–8824.

35 A. Schäfer, H. Horn and R. Ahlrichs, *J. Chem. Phys.*, 1992, **97**, 2571–2577.

36 A. Schäfer, C. Huber and R. Ahlrichs, *J. Chem. Phys.*, 1994, **100**, 5829–5835.

37 F. Weigend and R. Ahlrichs, *Phys. Chem. Chem. Phys.*, 2005, **7**, 3297–3305.

38 S. Grimme, J. Antony, S. Ehrlich and H. Krieg, *J. Chem. Phys.*, 2010, **132**, 154104.

39 F. Weigend, A. Köhn and C. Hättig, *J. Chem. Phys.*, 2002, **116**, 3175–3183.

40 C. Møller and M. S. Plesset, *Phys. Rev.*, 1934, **46**, 618–622.

41 F. Haase and R. Ahlrichs, *J. Comp. Chem.*, 1993, **14**, 907–912.

42 C. Hättig and F. Weigend, *J. Chem. Phys.*, 2000, **113**, 5154–5161.

43 C. Hättig, *J. Chem. Phys.*, 2003, **118**, 7751–7761.

44 C. Hättig, A. Hellweg and A. Köhn, *Phys. Chem. Chem. Phys.*, 2006, **8**, 1159–1169.

45 A. Hellweg, C. Hättig, S. Höfener and W. Klopper, *Theo. Chem. Acc.*, 2007, **117**, 587–597.

46 M. Gerenkamp and S. Grimme, *Chem. Phys. Letters*, 2004, **392**, 229–235.

47 D. Rappoport and F. Furche, *J. Chem. Phys.*, 2010, **133**, 134105.

48 F. Coester and H. Kümmel, *Nucl. Phys.*, 1960, **17**, 477 – 485.

49 J. Čížek, *J. Chem. Phys.*, 1966, **45**, 4256–4266.

50 R. J. Bartlett and M. Musiał, *Rev. Mod. Phys.*, 2007, **79**, 291–352.

51 D. P. Tew, W. Klopper, C. Neiss and C. Hättig, *Phys. Chem. Chem. Phys.*, 2007, **9**, 1921–1930.

52 H. Fliegl, W. Klopper and C. Hättig, *J. Chem. Phys.*, 2005, **122**, 084107.

53 T. Shiozaki, M. Kamiya, S. Hirata and E. F. Valeev, *J. Chem. Phys.*, 2008, **129**, 071101.

54 A. Köhn, G. W. Richings and D. P. Tew, *J. Chem. Phys.*, 2008, **129**, 201103.

55 C. Hättig, D. P. Tew and A. Köhn, *J. Chem. Phys.*, 2010, **132**, 231102.

56 P. Deglmann and F. Furche, *Chem. Phys. Letters*, 2002, **362**, 511–518.

57 O. Treutler and R. Ahlrichs, *J. Chem. Phys.*, 1995, **102**, 346.

58 C. Lee, W. Yang and R. G. Parr, *Phys. Rev. B*, 1988, **37**, 785–789.

59 J. Jusélius, D. Sundholm and J. Gauss, *J. Chem. Phys.*, 2004, **121**, 3952–3963.

60 D. Sundholm, H. Fliegl and R. J. Berger, *WIREs Comput. Mol. Sci.*, 2016, 639–678.

61 J. Ahrens, B. Geveci, C. Law, ParaView: An End-User Tool for Large Data Visualization, Visualization Handbook, Elsevier, 2005, ISBN-13: 978-0123875822, *see also: http://www.paraview.org*.

62 M. Dimitrova, H. Fliegl and D. Sundholm, *Phys. Chem. Chem. Phys.*, 2017, **19**, 20213–20223.

63 W. Humphrey, A. Dalke and K. Schulten, *J. Mol. Graphics*, 1996, **14**, 33–38.

64 GIMP: GNU Image Manipulation Program, *http://www.gimp.org*.

65 N. Jonathan, S. Gordon and B. P. Dailey, *J. Chem. Phys.*, 1962, **36**, 2443–2448.

66 H. J. Dauben Jr, J. D. Wilson and J. L. Laity, *J. Am. Chem. Soc.*, 1968, **90**, 811–813.

67 P. W. Fowler, E. Steiner, A. Acocella, L. W. Jenneskens and R. W. A. Havenith, *J. Chem. Soc., Perkin Trans. 2*, 2001, 1058–1065.

68 E. Steiner and P. W. Fowler, *J. Phys. Chem. A*, 2001, **105**, 9553–9562.

69 J.-i. Aihara and T. Horikawa, *Bull. Chem. Soc. Jpn.*, 1983, **56**, 1853–1854.

70 J.-i. Aihara and S. Oe, *Bull. Chem. Soc. Jpn.*, 2003, **76**, 1363–1364.

71 H. Fliegl, D. Sundholm, S. Taubert, J. Jusélius and W. Klopper, *J. Phys. Chem. A*, 2009, **113**, 8668–8676.

72 C. Gellini and P. Remigio Salvi, *Symmetry*, 2010, **2**, 1846–1924.

73 E. Matito, *ESI-3D: Electron Sharing Indices Program for 3D Molecular Space Partition*, http://ematito.webs.com/programs.htm.

74 A. Bondi, *J. Phys. Chem.*, 1964, **68**, 441–451.

75 B. Cordero, V. Gomez, A. E. Platero-Prats, M. Reves, J. Echeverria, E. Cremades, F. Barragan and S. Alvarez, *Dalton Trans.*, 2008, 2832–2838.

76 P. Pyykkö and M. Atsumi, *Chem. Eur. J.*, 2009, **15**, 186–197.